

Accumulation of ferromanganese crusts derived from carrier-free $^{10}\text{Be}/^{9}\text{Be}$

Lachner, J.; Ploner, M.; Steier, P.; Sakaguchi, A.; Usui, A.;

Originally published:

March 2020

Nuclear Instruments and Methods in Physics Research B 467(2020), 146-151

DOI: <https://doi.org/10.1016/j.nimb.2019.11.047>

Perma-Link to Publication Repository of HZDR:

<https://www.hzdr.de/publications/Publ-31927>

Release of the secondary publication
on the basis of the German Copyright Law § 38 Section 4.

CC BY-NC-ND

Accumulation of ferromanganese crusts derived from carrier-free $^{10}\text{Be}/^9\text{Be}$

Johannes Lachner, Marco Ploner, Peter Steier

University of Vienna, Isotope Research and Nuclear Physics, Währinger Str. 17, 1090 Wien, Austria

Aya Sakaguchi

University of Tsukuba, Tsukuba, 305-8577, Japan

Akira Usui

Kochi University, B200 Monobe, Nankoku, Kochi 783-8502, Japan

Abstract

The occurrence of ^{10}Be in natural archives is commonly used to date their formation and growth on time scales of million years. Accelerator Mass Spectrometry (AMS) can perform a direct measurement of the $^{10}\text{Be}/^9\text{Be}$ ratio. The carrier-free method, in which no ^9Be carrier is added to the original sample, is especially suitable for $^{10}\text{Be}/^9\text{Be}$ ratio determination in the marine environment. By normalizing the ^{10}Be content to ^9Be , temporal variations of Be uptake processes into the archive are eliminated.

Here, we present a simple method for the chemical extraction of beryllium from ferromanganese (FeMn) crusts or nodules, the measurement procedure, and the first carrier-free $^{10}\text{Be}/^9\text{Be}$ measurements at the 3 MV AMS facility VERA. Several tests of chemical methods are discussed including different options to short-cut and accelerate the procedure for special cases. Results from FeMn crust 237KD from cruise VA13/2 in the Pacific ocean show the known $^{10}\text{Be}/^9\text{Be}$ distribution with depth that is commonly related to a changing growth rate of the archive. In this context we discuss the potential influence of diffusion and adsorption processes on the age models of FeMn crusts that are based on radioactive nuclides such as ^{10}Be and ^{230}Th . Including an open-system behavior for these isotopes in the description of their profiles allows interpreting the accumulation of crusts with a constant growth rate over millions of years and does not require the assumption of abrupt growth changes.

Key words: ^{10}Be , carrier-free $^{10}\text{Be}/^9\text{Be}$, AMS, VERA, ferromanganese crusts

1. Introduction

Dating environmental archives on the time-scale of several million years can be accomplished using the long-lived radioisotope ^{10}Be ($T_{1/2}=1.39$ Myr, Korschinek et al. (2010); Chmeleff et al. (2010)). The use of the $^{10}\text{Be}/^9\text{Be}$ ratio in dating assumes that ^{10}Be follows ^9Be during incorporation into an archive and that there has been a constant initial isotopic concentration over the time of formation without subsequent isotopic exchange. While ^{10}Be is primarily produced in the atmosphere by spallation reactions of cosmic rays, ^9Be is abundant in the lithosphere and from there

is transferred into aqueous media via erosion. In the ocean water no variations of ^9Be due to changing weathering input are detected over the last 10 Myr (Willenbring and von Blanckenburg, 2010), i.e. ^9Be is suitable to compensate for any effects caused by a potential temporal variability in the Be uptake process into an archive. Therefore, the $^{10}\text{Be}/^9\text{Be}$ ratio can be assumed to be more robust than the ^{10}Be concentration alone.

In order to measure $^{10}\text{Be}/^9\text{Be}$ ratios it is crucial to determine minute amounts of the long-lived ^{10}Be and the stable ^9Be without introducing any contamination for either of the two isotopes. There are few carrier-free approaches, measuring $^{10}\text{Be}/^9\text{Be}$ with SIMS (von Blanckenburg et al., 1996a) or AMS (Maden et al., 2004). Alternatively, the $^{10}\text{Be}/^9\text{Be}$ ratio is determined by combination of an AMS measurement and a suitable mass-spectrometric determination of ^9Be concentration. In that case a conventional AMS measurement is conducted using several $100\mu\text{g}$ of ^9Be carrier and diluting the natural $^{10}\text{Be}/^9\text{Be}$ ratios that typically range from 10^{-7} to 10^{-11} by ≈ 3 orders of magnitude. The additional measurement of the natural ^9Be content in the sample is typically carried out with ICP-OES (Graham et al., 2004), AAS (Ménabréaz et al., 2012) or ICP-MS (Feige et al., 2013).

Disadvantages of the carrier-free method comprise the necessity to determine very low ^9Be currents and that direct information on the ^{10}Be concentration of the sample is not available without a further independent determination of the ^9Be concentration in the sample.

In an application such as the dating of a marine archive, however, where the $^{10}\text{Be}/^9\text{Be}$ ratio is the quantity of interest, the great advantage of the carrier-free method is that only one measurement, i.e. the AMS measurement, is required. This advantage is reinforced by the fact that the determination of the stable ^9Be concentration in a sample aliquot is challenging and seems to be easily affected e.g. by matrix effects (Merchel et al., 2013).

FeMn crusts are compact archives spanning periods of several half-lives of ^{10}Be and thus are a suitable material to apply the carrier-free Be method. They exist only in oxidizing environments without sedimentation and accumulate material by precipitation from ocean water which results in slow growth rates of few mm/Myr. They reach total thicknesses of some centimeter. For dating these archives on short periods (< 1 Myr) $^{230}\text{Th}_{\text{ex}}$ is used (Eisenhauer et al., 1992); on longer time ranges than quantifiable with ^{10}Be this can be performed with Os isotopes (Klemm et al., 2005). Alternatively, a magnetostratigraphic technique also shows results consistent with $^{10}\text{Be}/^9\text{Be}$ dating (Oda et al., 2011; Noguchi et al., 2017). In any case, the closed-system conditions for the element used to establish an age model are a fundamental requirement and highly mobile species such as uranium, for which open-system conditions in FeMn crusts have been documented (Neff et al., 1999), are not qualified.

2. Materials and AMS setup

2.1. Target materials and chemical preparation

FeMn crusts are mainly composed of oxides of Fe and Mn (for 237KD from cruise VA13/2 $C_{\text{Fe}} = 17.5\%$ and $C_{\text{Mn}} = 23.9\%$, Eisenhauer et al. (1992)) with abundances of Na, Mg, Al, Ca in the range of a few percent. In contrast to those rather abundant elements the Be concentration usually amounts to several $\mu\text{g/g}$. With sample amounts of

10-150 mg this leaves us with some 10 to some 100 ng of ^9Be for the analysis. During the cruise VA13/2 the crust sample 237KD was recovered at $09^\circ 25' \text{ N}$, $146^\circ 03' \text{ W}$ from 4830 m water depth. It has a thickness of up to 40 cm and has been previously dated using ^{10}Be (Segl et al., 1984; Segl et al., 1984) and ^{230}Th (Eisenhauer et al., 1992). Furthermore, it has been used to derive the interstellar/Supernova ^{60}Fe signal (Knie et al., 2004). For this crust a change in elemental composition is reported at an age of 13 Myr (Frank et al., 1999).

The applied chemical procedure (Fig. 1) consisted of dissolution of the original material with subsequent column chemistry and a final coprecipitation in an Fe_2O_3 matrix, following previously described routines for the extraction of the authigenic Be from FeMn crusts or marine sediments (von Blanckenburg et al., 1996a; Lachner et al., 2013). The obtained material was pressed into Al cathodes. Targets used for tuning the machine consist of $\leq 1 \mu\text{g}$ Be in 2 mg Fe_2O_3 . Chemistry blanks to study the entry of either ^9Be or ^{10}Be into the procedure were produced by using all chemicals required for the Be extraction without an original sample.

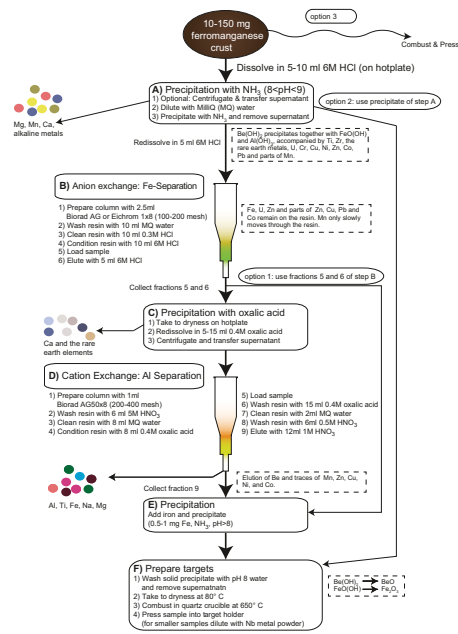


Figure 1: Schematic of the chemical procedure including options to short-cut the multi-step column chemistry.

The main component of the final carrier-free Be target is the Fe_2O_3 matrix, which dilutes the concentrated ^9Be so that the targets last long enough during the measurement. As an alternative to the strong chemical pre-concentration followed by a controlled dilution we tested several options to reduce the chemical efforts or even to use the FeMn crust directly. Previous experiments on the extraction of Be from natural samples indicated that there are no negative influences of remainders of Al or Ti above a simple dilution effect (Merchel et al., 2008). For this reason, various steps of the chemical procedure were omitted and three different options of a reduced chemistry were studied. In this project thirteen samples were prepared from the crust 237KD retrieved by the cruise VA13/2. Four samples underwent short

versions of the chemical procedure. Several samples were from material with an independently determined $^{10}\text{Be}/^9\text{Be}$ ratio (Usui et al., 2007, 2017).

2.2. AMS setup

For ^{10}Be measurements the AMS system VERA (e.g. Steier et al. (2004)) is operated at a terminal voltage of the pelletron accelerator of 3 MV along with stripping to the 2+ charge state. High transmission through the accelerator and sufficient energy for isobar suppression ($E = 7.18 \text{ MeV}$) can be combined. The detection of $^{10}\text{Be}^{2+}$ is carried out in a gas ionization chamber with a passive absorber consisting of a foil stack of SiN foils to stop the isobar ^{10}B (Steier et al., 2019). Due to the lower ^9Be content in the sample the interference from $^9\text{BeH}^{2+}$ molecules in the detector is largely reduced compared to conventional measurements.

2.3. Beam transport

The BeO^- extraction from the Fe_2O_3 target matrix is very efficient: In combination with the good transmission from the low energy side into the ionization chamber it enables us to detect more than 0.1% of the total material during the first hour of sputtering a target. Test samples containing a known amount of BeO show an output corresponding to a BeO^- formation efficiency of 2% over a sputtering time of 2.5 h. Charge exchange in the stripper has been tested for Ar and He resulting in optimal conditions (55%) for Ar stripping to the Be^{2+} state at a terminal voltage of 3 MV and a lower maximum value (42%) for stripping with He gas. In contrast to the conventional ^{10}Be measurements it is not required to raise the stripper gas pressure in order to suppress surviving $^9\text{BeH}^{2+}$ molecules. The lower intensity of $^9\text{BeH}^{2+}$ from the carrier-free samples allows for operation at the pressure with optimum yield for the 2+ charge state. This slightly improves the measurement yield for the carrier-free method. For a stable measurement of the pA-nA ^9Be currents a longer integration time is required and takes up $\approx 6\%$ of the measurement time. By positioning the detector after a magnetic quadrupole allowing for optimal focusing of the beam through the 5 mm-5 mm absorber foil stack the $^{10}\text{Be}^{2+}/^9\text{Be}^{2+}$ ratio of the standards is measured at 80% of the nominal value. The losses of ^{10}Be relative to ^9Be are partially explained by the tight counting bin, while additional processes are still under discussion (Steier et al., 2019).

Within 2.5 hours an overall efficiency of 0.8% for ^{10}Be detection can be reached. On the whole, there is no major difference in efficiency for ^{10}Be detection from carrier-free samples compared to a conventional determination.

3. Results

3.1. Chemical yield

After a full chemical procedure the currents of real samples range from 0.5 to 15 nA $^9\text{Be}^{16}\text{O}^-$. At the same time the level of blanks for ^9Be currents amounts to 10-25 pA with a ^{10}Be counting rate $0.01\text{-}0.1 \text{ s}^{-1}$. This introduction of ^9Be into the sample, which is monitored via the chemistry blanks, corresponds to additional 5 pg Be in the original material. Typically, traditional carrier-added targets exhibit $^9\text{Be}^{16}\text{O}^-$ currents of $1 \mu\text{A}$ (Steier et al., 2019).

Previous $^{10}\text{Be}/^9\text{Be}$ measurements of the same material with conventional AMS (Fig. 2) and double preparations of the same material and measurement in different carrier-free beam times produce $^{10}\text{Be}/^9\text{Be}$ results that are consistent within 5% for $^{10}\text{Be}/^9\text{Be}$ ratios $\geq 10^{-9}$.

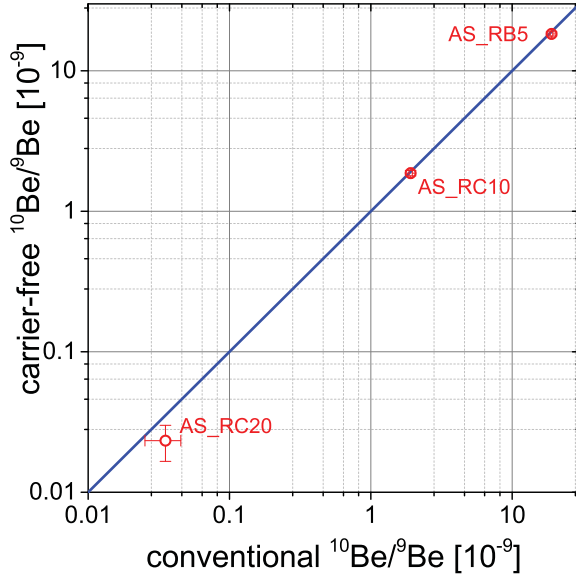


Figure 2: Comparison between $^{10}\text{Be}/^9\text{Be}$ ratios determined with the carrier-free method at VERA and previous results (Usui et al., 2007, 2017) on the same material.

Relative to a direct use of the raw FeMn crust material after combusting it at 650°C an improvement of the output by a factor ≈ 5 (Fig. 3) can be accomplished by performing at least option 2 of the chemical separation (Fig. 1), i.e. the dissolution of FeMn material with a subsequent Fe hydroxide coprecipitation. Using option 1 a further factor ≈ 3 can be gained by including the steps with the first column and the subsequent coprecipitation with added Fe solution. Still, relative to the full chemistry another factor ≥ 4 is missing. These differences are related to the greater concentration of the samples if the full chemistry is performed. Furthermore, better purification of the material changes the composition of the AMS target, e.g. removing compounds with poor electric and thermal conductivity, and may increase the yield of the BeO^- current. The different options show no major effect on the ^{10}B intensity, which was measured for the different targets as the $^{10}\text{B}^{2+}$ current in a Faraday cup directly in front of the detector at 5-50 pA.

While the relative uncertainty for the $^{10}\text{Be}/^9\text{Be}$ ratio increased for the targets with reduced chemical treatment because of the lower ^{10}Be counting rate, the ratios are in good agreement (Fig. 3). Short-cutting the chemical procedure thus is an alternative for a quick screening of a large number of samples where precision dating is not required. With the reduced Be content in the AMS target and the lower Be output of the sample uncertainties are higher by a factor of two due to the lower counting statistics.

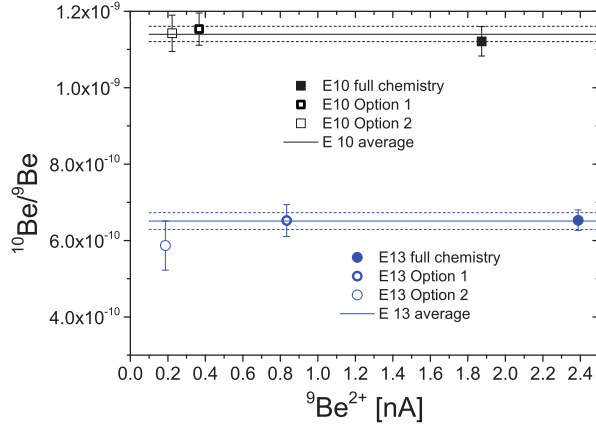


Figure 3: Short-cutting the chemical procedure results in lower ${}^9\text{Be}$ currents but gives consistent results for the ${}^{10}\text{Be}/{}^9\text{Be}$ ratio.

3.2. Cross contamination

In a measurement sequence of blanks and high standards we also determined the cross-contamination for ${}^{10}\text{Be}$ in our ion source (type MC-SNICS, NEC, Middleton, USA). The cross-contamination for Be in the ion source is modeled depending on the rate and measurement time of standards and on the period between standard and blank measurement. For measurement parameters and sample run times during routine operation this results in a typical cross-contamination $\frac{{}^{10}\text{Be}/{}^9\text{Be}_{\text{blank}}}{{}^{10}\text{Be}/{}^9\text{Be}_{\text{standard}}} \approx 5 \cdot 10^{-5}$. While continuously sputtering a sample the cross-contamination decreases roughly exponentially with a half-life of ≈ 35 minutes.

3.3. FeMn crust samples

The typical surface samples of FeMn crusts or nodules show values of ${}^{10}\text{Be}/{}^9\text{Be} \approx 10^{-7}$ and exhibit present-day ratios of ocean bottom water (von Blanckenburg et al., 1996b). The lowest crust sample in our study yielded a ratio of ${}^{10}\text{Be}/{}^9\text{Be} \approx (2.3 \pm 0.7) \cdot 10^{-11}$. From the decay law one may thus derive a dating range of at least ≈ 12 half-lives or 17 Myr. Even with a 30% measurement uncertainty for the lowest ratio this results in a relatively small dating uncertainty of 5% (≈ 1 Myr) if one can assume a strict abundance by the decay law. The assumption of a constant initial ${}^{10}\text{Be}/{}^9\text{Be}$ ratio has to be tested over those timescales with an independent dating method.

4. Modeling ${}^{10}\text{Be}/{}^9\text{Be}$ ratios in FeMn crusts

The common interpretation for a kink in the ${}^{10}\text{Be}/{}^9\text{Be}$ ratio over depth (e.g. at ca. 15 mm in Fig. 4) is a changing growth rate G of the FeMn crust. Assuming a closed-system behavior of Be in the crust one can derive growth rates of 2.62 ± 0.08 mm/Ma for the top 12 mm of the crust and 4.08 ± 0.24 mm/Ma deeper than 12 mm or before 4.5 Myr from the presented data of crust 237KD. This estimation of the growth rates does not include the slightly lowered surface data point measured with the carrier free method. Such an inversion (Kusakabe and Ku, 1984) or a flattening (Mangini et al., 1986) has been previously reported for the ${}^{10}\text{Be}/{}^9\text{Be}$ ratio in the top mm of FeMn crusts. However,

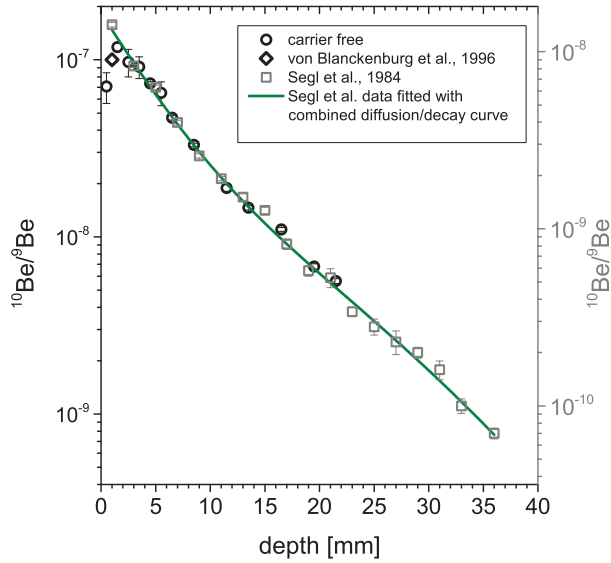


Figure 4: Carrier-free $^{10}\text{Be}/^9\text{Be}$ results (left axis) for crust 237KD VA13/2 from the central Pacific are compared with literature data (left axis: von Blanckenburg et al. (1996b), right axis: Segl et al. (1984)). The right axis is shifted by a constant factor (1/9) relative to the right axis. Both data sets show a decrease over depth that cannot be explained with a simple exponential decay of ^{10}Be at constant growth rate. Model predictions for a constant growth rate with Be mobility according to equation 2.

no similar surface behavior was observed in the previous $^{10}\text{Be}/^9\text{Be}$ determination of the same crust (Fig. 4, Segl et al. (1984)). Therefore, a surface contamination of our FeMn crust sample with ^9Be could also be an explanation. In the comparison with Segl et al. (1984) a factor of ≈ 9 difference between the two $^{10}\text{Be}/^9\text{Be}$ data sets is striking. A third independent measurement of a top crust sample from cruise VA13/2 (von Blanckenburg et al., 1996b) gives a $^{10}\text{Be}/^9\text{Be}$ ratio of $1.0 \cdot 10^{-7}$ and thus is compatible with the carrier-free data set rather than with the conventional measurement. Therefore, we presume that the factor might come from a systematic offset in the ^9Be determination of Segl et al. (1984). Apart from this, the presented growth rates are in agreement with the previously derived values for the same crust if one corrects for the updated value of the ^{10}Be half-life (Korschinek et al., 2010; Chmeleff et al., 2010). Segl et al. (1984) related the change of growth rate to a change in ocean circulation patterns transporting less Fe and Mn to the growth site of the crust and thus leading to slower accumulation.

If one relaxes the requirement of a closed-system behavior of Be in the crust, an alternative explanation of the kink in the $^{10}\text{Be}/^9\text{Be}$ ratio over depth is conceivable: Crusts exhibit a porous structure with mean porosity of 60% (Hein et al., 2003). These pores are filled with seawater so that the deeper layers in the crusts are presumably connected to the surface. Therefore, any chemical exchange between the crust and the pore fluid leads to a mobile behavior, e.g. diffusion of ions and subsequent adsorption to the crust, effectively removing ions from the pore fluid. An additional input of the radioactive isotope creates the appearance of a younger age for deeper material.

Models taking into account both diffusion and radioactive decay exist since the earliest studies of U isotopes and ^{10}Be in FeMn crusts (Ku et al., 1979). A mobile and open-system behavior inside FeMn crusts was observed

for soluble species such as U (Neff et al., 1999; Henderson and Burton, 1999). The diffusion in the pore water and mobility between the fluid and solid phase of the crust is documented for depths up to 6 mm. Processes including Be exchange between the fluid and the solid phase are not sufficient to explain the effects observed in FeMn crusts if one exclusively considers Be that is primarily incorporated into the crust's top layer and later remobilized into the liquid phase: Based on the estimations of Be mobility deduced from U mobility by Henderson and Burton (1999) the ^{10}Be decay curve should be disturbed by $< 1\%$ on timescales of 30 Myr. Instead of only redistributing incorporated Be by diffusion, processes of adsorption from the fluid to the solid phase in the highly porous crust material may have to be considered for the incorporation together with continuous input from the ocean bottom water to the pore water of the crust (Kusakabe and Ku, 1984). In such post-depositional diagenesis some of the Be dissolved in the ocean water is directly transported via the pore water into greater depth of the crust and incorporated there.

Incorporation of ^{10}Be from the pore water into the FeMn crust (growth rate $G = 1/\mu\tau$, τ as the radionuclide's mean lifetime) can be included by the addition of a depth-dependent production term p to the normal decay equation:

$$dN(x)/dx = -\mu \cdot N(x) + p(x) \quad (1)$$

In general, diffusion processes will produce a depth and time dependent production term $p = p(x, t)$. We assume a constant growth rate and introduction from the surface to depth with a function $p(x) = p_0 \cdot (1 - \text{erf}(x/x_D))$, which is derived from the solution of the differential diffusion equation. The diffusion length x_D states to which depth the radionuclide diffused during time t and is connected with the effective diffusivity D_{eff} by $x_D = 2\sqrt{D_{eff}t}$. The surface boundary condition is $N(0) = N_0 + p_0/\mu$, where the first term describes the contribution by direct fixation of Be at the boundary and the second term gives the input of the mobile component to the top layer. Then, the differential equation 1 is solved by

$$N(x) = N_0 \cdot e^{-\mu x} + \frac{p_0}{\mu} \cdot (1 - \text{erf}(x/x_D)) + \frac{p_0}{\mu} \cdot e^{-\mu x} \cdot \left(e^{\mu^2 x_D^2/4} \cdot (\text{erf}(\mu x_D/2) - \text{erf}(\mu x_D/2 - x/x_D)) \right). \quad (2)$$

The depth profile can be described by equation 2, which has four free parameters N_0 , μ , p_0 , and x_D . If this equation is fitted to the depth profile shown in Fig. 4, it yields a (constant) growth rate $G=2.0\pm0.1$ mm/Myr. In this case, the contribution from post-depositional addition of ^{10}Be (2nd and 3rd terms in eqn. 2 with parameter p_0) is found to exceed the original component (1st term with parameter N_0) for depths greater than 10 mm.

With the presented scenario of continuous adsorption of Be into the crust at a constant ^9Be concentration in the seawater one has to expect also an increased ^9Be concentration with depth. At least for the crust 237KD the ^9Be concentration data (Segl et al., 1984) shows such a trend and thus is in agreement with an additional input of dissolved ions into the crust over time.

Sensitive measurements of other natural or anthropogenic radioactive isotopes with different half-lives could be of eminent help to explain the behavior of the $^{10}\text{Be}/^9\text{Be}$ ratio:

Highly-resolved ^{230}Th ($T_{1/2} = 75$ kyr) data in the top 1.4 mm of the same crust 237KD VA13/2 (Eisenhauer et al., 1992) show a decrease of the concentration only after a rather flat behavior in the top ≈ 0.2 mm as shown in Fig. 5. This set of data was interpreted as an exponential decay curve showing a growth rate of ≈ 6 mm/Myr for the investigated region, i.e. the recent 200 kyr, which disagreed with the lower growth rates derived from ^{10}Be at greater depths in the crust. This disagreement was explained in terms of a recent change in the accumulation rate of the crust. Similarly, discordant $^{230}\text{Th}_{exc}$ and ^{10}Be data for a number of FeMn nodules have also been interpreted as recent changes in growth rate (Krishnaswami et al., 1982).

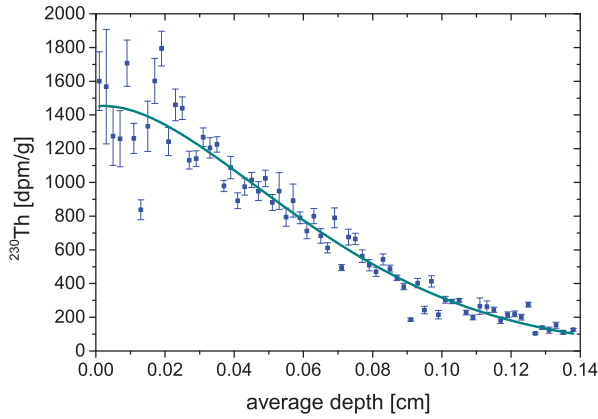


Figure 5: ^{230}Th concentrations as a function of depth for the same crust as studied in the present work (237KD from cruise VA13/2) from the central Pacific over depth (Eisenhauer et al., 1992). The solid line is a fit based on equation 2 using the growth rate $G=2.0$ mm/Myr that was derived from ^{10}Be to define the parameter μ .

If, on the other hand, we use the model of a combined exponential decay and a diffusional input with post-depositional fixation (eq. 2) the data for crust 237KD from cruise VA13/2 (Eisenhauer et al., 1992) can be equally well described assuming the ^{10}Be derived growth rate and a dominant additional input of ^{230}Th via incorporation of dissolved Th into the crust (Fig. 5). This would mean that in this case the ^{230}Th concentration does not give direct information on the age. Thereby, the disagreement of the ^{10}Be and ^{230}Th data can be resolved so that the recent change of the growth rates may be unnecessary in order to bring both data sets into accordance.

The age model might be expanded using ^{53}Mn ($T_{1/2}=3.7$ Myr, Honda and Imamura (1971)) measurements. Data from the same crust 237KD (Poutivtsev, 2007) are available but the uncertainties are too high to distinguish between different growth scenarios of the crust. The ^{53}Mn data were described by a constant growth of the crust at a rate of $\approx 2.5 \pm 0.2$ mm/Myr over the first 3 cm, which could mean a mobile behavior of ^{10}Be in the crust. However, a changing growth rate at a depth of 10-12 mm was also compatible with the same data set (Poutivtsev, 2007).

In the case of ^{26}Al , a similar mobility of Al and Be would result in a stronger influence on the distribution. Due to the shorter half-life of 0.7 Myr the ^{26}Al concentration decays faster over depth and a transport of ^{26}Al from surface

thus may create an impact already at shallower depths than for ^{10}Be . However, in the case of ^{26}Al one also has to consider the additional production via the reaction $^{23}\text{Na}(\alpha, n)^{26}\text{Al}$, depending on the α flux from $^{230,232}\text{Th}$ and ^{238}U decay (Feige, 2014), which also depends on depth in the crust.

Profiles of anthropogenic fission products, e.g. ^{90}Sr , with a depth dependence that can be explained by input via diffusion would serve as a fingerprint for a non-closed system behavior. Similarly, the detection of radionuclides that are of unambiguous anthropogenic origin, e.g. ^{238}Pu or ^{240}Pu , in greater depths of FeMn crusts would indicate post-depositional addition of material.

In contrast to the radionuclides discussed above, the $^{187}\text{Os}/^{188}\text{Os}$ isotope system is not primarily governed by radioactive decay. ^{187}Os is a daughter of the long-lived ^{187}Re with a half-life of 46 Gyr and thus is continuously produced. However, the input of ^{187}Os to the ocean, which is mainly by continental weathering (Sharma et al., 1997), has found to be not continuous (Pegram and Turekian, 1999). Therefore, relative dating up to 80 Myr can be performed by identifying a common pattern of $^{187}\text{Os}/^{188}\text{Os}$ in archives. The measured $^{187}\text{Os}/^{188}\text{Os}$ in the archive is adjusted to the known seawater curve over time in order to get a depth-age relationship. This can help in the identification of growth-rate changes or hiatuses (Klemm et al., 2005; Goto et al., 2017). It is advantageous for this method that it is not based on a strong gradient in the isotopic ratio: Os mobility would wash out the original signature but may not necessarily shift the age model towards younger ages. For all radionuclides, a mobile behavior leads to apparent younger ages of the crust in greater depths. The determination of the Os isotopic ratio therefore may give valuable complementary information on the age model of old FeMn crusts.

5. Conclusion

Measuring $^{10}\text{Be}/^9\text{Be}$ ratios is a powerful tool to date marine deposits in the time range of million years. The method is applicable for marine sediments but also for ferromanganese (FeMn) crusts with growth rates of only few mm/Myr, which are of special interest for geochemical and even astrophysical studies. The low abundance of Be in natural materials poses challenges to the preparation of samples and to very sensitive measurements of both ^{10}Be and ^9Be : The presented procedure to separate Be from the matrix works for sample sizes of 10-100 mg FeMn crust containing less than $1\text{ }\mu\text{g }^9\text{Be}$ and results in Be currents in the range of several 100 pA to few nA. Options of shortening and simplifying the carrier-free method make it suitable for both quick large-scale surveys with many samples and highly sensitive determination of low natural $^{10}\text{Be}/^9\text{Be}$ ratios.

Conventional radiometric dating of FeMn crusts uses a closed system behavior and changes in the $^{10}\text{Be}/^9\text{Be}$ curve then can be attributed to a change in the growth rate. The model introduced in this work shows an alternative interpretation of the depth profile of radioactive nuclei in a crust on the basic assumption of a constant growth rate but including a depth dependent input. Still, age information can be obtained from the $^{10}\text{Be}/^9\text{Be}$ data.

High-resolution isotopic data of different systems such as the discussed $^{10}\text{Be}/^9\text{Be}$, $^{53}\text{Mn}/^{55}\text{Mn}$, $^{187}\text{Os}/^{188}\text{Os}$, $^{230}\text{Th}_{\text{ex}}$ or of anthropogenic nuclides are required to assess the growth of FeMn crusts, to investigate a potential mobile be-

havior of Be in the FeMn crust, and to put stronger limits on models describing post-depositional diagenesis. For a better understanding of the pore water interaction with the solid phase of the FeMn crust and of effects from diffusion or accretion of elements the evaluation of multiple isotopic systems in crusts with different porosities and growth histories will be very helpful.

Acknowledgements

We are very grateful to Kosuke Goto for helpful discussions on the Os isotopic signature and to Marcus Christl for bringing to our notice the past works on U mobility in FeMn crusts. The comments of an anonymous reviewer are also gratefully acknowledged.

References

- G. Korschinek, A. Bergmaier, T. Faestermann, U. Gerstmann, K. Knie, G. Rugel, A. Wallner, I. Dillmann, G. Dollinger, C. L. von Gostomski, K. Kossert, M. Maiti, M. Poutivtsev, A. Remmert, A new value for the half-life of ^{10}Be by Heavy-Ion Elastic Recoil Detection and liquid scintillation counting, *Nucl. Instrum. Meth. B* 268 (2) (2010) 187 – 191.
- J. Chmeleff, F. von Blanckenburg, K. Kossert, D. Jakob, Determination of the ^{10}Be half-life by multicollector ICP-MS and liquid scintillation counting, *Nucl. Instrum. Meth. B* 268 (2) (2010) 192–199.
- J. Willenbring, F. von Blanckenburg, Long-term stability of global erosion rates and weathering during late-Cenozoic cooling, *Nature* 465 (2010) 211 – 214.
- F. von Blanckenburg, N. Belshaw, R. O’Nions, Separation of ^9Be and cosmogenic ^{10}Be from environmental materials and SIMS isotope dilution analysis, *Chem. Geology* 129 (1-2) (1996a) 93 – 99.
- C. Maden, M. Döbeli, P. W. Kubik, M. Frank, M. Suter, Measurement of carrier-free ^{10}Be samples with AMS: the method and its potential, *Nucl. Instrum. Meth. B* 223-224 (2004) 247–252.
- I. Graham, R. Carter, R. Ditchburn, A. Zondervan, Chronostratigraphy of ODP 181, Site 1121 sediment core (Southwest Pacific Ocean), using $^{10}\text{Be}/^9\text{Be}$ dating of entrapped ferromanganese nodules, *Marine Geology* 205 (1-4) (2004) 227 – 247.
- L. Ménabréaz, D. L. Bourlès, N. Thouveny, Amplitude and timing of the Laschamp geomagnetic dipole low from the global atmospheric ^{10}Be overproduction: Contribution of authigenic $^{10}\text{Be}/^9\text{Be}$ ratios in west equatorial Pacific sediments, *J. Geophys. Res.: Solid Earth* 117 (2012) B11101.
- J. Feige, A. Wallner, L. Fifield, Korschinek, G., Merchel, S., Rugel, G., Steier, P., Winkler, S.R., Golser, R., AMS measurements of cosmogenic and supernova-ejected radionuclides in deep-sea sediment cores, *EPJ Web of Conferences* 63 (2013) 03003.
- S. Merchel, W. Bremser, D. L. Bourlès, U. Czeslik, J. Erzinger, N.-A. Kummer, L. Leanni, B. Merkel, S. Recknagel, U. Schaefer, Accuracy of ^9Be -data and its influence on ^{10}Be cosmogenic nuclide data, *J. Radioanal. Nucl. Chem.* 298 (2013) 1871 – 1878.
- A. Eisenhauer, K. Gögen, E. Pernicka, A. Mangini, Climatic influences on the growth rates of Mn crusts during the Late Quaternary, *Earth Planet. Sci. Lett* 109 (1) (1992) 25 – 36.
- V. Klemm, S. Levasseur, M. Frank, J. R. Hein, A. N. Halliday, Osmium isotope stratigraphy of a marine ferromanganese crust, *Earth Planet. Sc. Lett.* 238 (1) (2005) 42 – 48.
- H. Oda, A. Usui, I. Miyagi, M. Joshima, B. P. Weiss, C. Shantz, L. E. Fong, K. K. McBride, R. Harder, F. J. Baudenbacher, Ultrafine-scale magnetostratigraphy of marine ferromanganese crust, *Geology* 39 (2011) 227–230.
- A. Noguchi, H. Oda, Y. Yamamoto, A. Usui, M. Sato, J. Kawai, Scanning SQUID microscopy of a ferromanganese crust from the northwestern Pacific: Submillimeter scale magnetostratigraphy as a new tool for age determination and mapping of environmental magnetic parameters, *Geophys. Res. Lett.* 44 (2017) 5360–5367.

277 U. Neff, A. Bollhöfer, N. Frank, A. Mangini, Explaining discrepant depth profiles of $^{234}\text{U}/^{238}\text{U}$ and $^{230}\text{Th}_{\text{ex}}$ in Mn-crusts, *Geochim. et Cosmochim.*
 278 *Acta* 63 (15) (1999) 2211 – 2218.

279 M. Segl, A. Mangini, G. Bonani, H. Hofmann, M. Nessi, M. Suter, W. Wölfli, G. Friedrich, W. Plünger, A. Wiechowski, J. Beer, ^{10}Be -dating of a
 280 manganese crust from Central North Pacific and implications for ocean palaeocirculation, *Nature* 309 (7) (1984) 540 – 543.

281 M. Segl, A. Mangini, G. Bonani, H. Hofmann, E. Morenzoni, M. Nessi, M. Suter, W. Wölfli, ^{10}Be dating of the inner structure of Mn-encrustations
 282 applying the Zürich tandem accelerator, *Nucl. Instrum. Meth. B* 5 (2) (1984) 359 – 364.

283 K. Knie, G. Korschinek, T. Faestermann, E. A. Dorfi, G. Rugel, A. Wallner, ^{60}Fe Anomaly in a Deep-Sea Manganese Crust and Implications for a
 284 Nearby Supernova Source, *Phys. Rev. Lett.* 93 (17) (2004) 171103.

285 M. Frank, R. O’Nions, J. Hein, V. Banakar, 60 Myr records of major elements and Pb-Nd isotopes from hydrogenous ferromanganese crusts:
 286 reconstruction of seawater paleochemistry, *Geochim. Cosmochim. Acta* 63 (11) (1999) 1689 – 1708.

287 J. Lachner, M. Christl, H.-A. Synal, M. Frank, M. Jakobsson, Carrier free $^{10}\text{Be}/^{9}\text{Be}$ measurements with low-energy AMS: Determination of
 288 sedimentation rates in the Arctic Ocean, *Nucl. Instrum. Meth. B* 294 (0) (2013) 67 – 71.

289 S. Merchel, M. Arnold, G. Aumaitre, L. Benedetti, D. Bourles, R. Braucher, V. Alfimov, S. Freeman, P. Steier, A. Wallner, Towards more precise
 290 ^{10}Be and ^{36}Cl data from measurements at the 10^{-14} level: Influence of sample preparation, *Nucl. Instrum. Meth. B* 266 (22) (2008) 4921 –
 291 4926.

292 A. Usui, I. J. Graham, R. G. Ditchburn, A. Zondervan, H. Shibasaki, H. Hishida, Growth history and formation environments of ferromanganese
 293 deposits on the Philippine Sea Plate, northwest Pacific Ocean, *Island Arc* 16 (2007) 420–430.

294 A. Usui, K. Nishi, H. Sato, Y. Nakasato, B. Thornton, T. Kashiwabara, A. Tokumaru, A. Sakaguchi, K. Yamaoka, S. Kato, S. Nitahara, K. Suzuki,
 295 K. Iijima, T. Urabe, Continuous growth of hydrogenetic ferromanganese crusts since 17Myr ago on Takuyo-Daigo Seamount, NW Pacific, at
 296 water depths of 800-5500m, *Ore Geology Reviews* 87 (2017) 71–87.

297 P. Steier, R. Golser, W. Kutschera, A. Priller, C. Vockenhuber, S. Winkler, VERA, an AMS facility for all isotopes, *Nucl. Instrum. Meth. B* 223-224
 298 (2004) 67–71.

299 P. Steier, M. Martschini, J. Buchriegler, J. Feige, J. Lachner, S. Merchel, L. Michlmayr, A. Priller, G. R. E. Schmidt, A. Wallner, E. M. Wild,
 300 R. Golser, Comparison of methods for the detection of ^{10}Be with AMS and a new approach based on a silicon nitride foil stack, *Int. J. Mass*
 301 *Spectrom.* 444 (2019) 116175.

302 F. von Blanckenburg, R. O’Nions, N. Belshaw, A. Gibb, J. Hein, Global distribution of beryllium isotopes in deep ocean water as derived from
 303 Fe-Mn crusts, *Earth and Planetary Science Letters* 141 (1-4) (1996b) 213 – 226.

304 M. Kusakabe, T.-L. Ku, Incorporation of Be isotopes and other trace metals into marine ferromanganese deposits, *Geochim. Cosmochim. Acta*
 305 48 (11) (1984) 2187–2193.

306 A. Mangini, M. Segl, H. Kudrass, M. Wiedicke, G. Bonani, H. Hofmann, E. Morenzoni, M. Nessi, M. Suter, W. Wölfli, Diffusion and supply
 307 rates of ^{10}Be and ^{230}Th radioisotopes in two manganese encrustations from the South China Sea, *Geochim. Cosmochim. Acta* 50 (1) (1986)
 308 149–156.

309 J. Hein, A. Koschinsky, M. Bau, F. Manheim, J.-K. Kang, L. Roberts, Cobalt-rich ferromanganese crusts in the Pacific, in: D. Cronan (Ed.),
 310 *Handbook of Marine Mineral Deposits*, CRC Press, Boca Raton, Florida, 239–279, 2003.

311 T. Ku, A. Omura, P. Chen, Be10 and U-Series Isotopes in Manganese Nodules from the Central North Pacific, *Marine Geology and Oceanography*
 312 *of the Pacific Manganese Nodule Province. Marine Science* 9 (1979) 791–814.

313 G. M. Henderson, K. W. Burton, Using ($^{234}\text{U}/^{238}\text{U}$) to assess diffusion rates of isotope tracers in ferromanganese crusts, *Earth Planet. Sc. Lett.*
 314 170 (3) (1999) 169 – 179.

315 S. Krishnaswami, A. Mangini, J. Thomas, P. Sharma, J. Cochran, K. Turekian, P. Parker, ^{10}Be and Th isotopes in manganese nodules and adjacent
 316 sediments: Nodule growth histories and nuclide behavior, *Earth Planet. Sci. Lett.* 59 (2) (1982) 217–234.

317 M. Honda, M. Imamura, Half-life of ^{53}Mn , *Phys. Rev. C* 4 (1971) 1182–1188.

318 M. Poutivtsev, Extraterrestrisches ^{53}Mn in hydrogenetischen Mangankrusten, Ph.D. thesis, TU München, 2007.

319 J. Feige, Supernova-Produced Radionuclides in Deep-Sea Sediments Measured with AMS, Ph.D. thesis, Dissertation University Vienna, 2014.

- 320 M. Sharma, D. Papanastassiou, G. Wasserburg, The concentration and isotopic composition of osmium in the oceans, *Geochimica et Cosmochimica*
321 *Acta* 61 (1997) 3287–3299.
- 322 W. J. Pegram, K. K. Turekian, The osmium isotopic composition change of Cenozoic sea water as inferred from a deep-sea core corrected for
323 meteoritic contributions, *Geochimica et Cosmochimica Acta* 63 (1999) 4053–4058.
- 324 K. T. Goto, T. Nozaki, T. Toyofuku, A. H. Augustin, G. Shimoda, Q. Chang, J. Kimura, K. Kameo, H. Kitazato, K. Suzuki, Paleocceanographic
325 conditions on the São Paulo Ridge, SW Atlantic Ocean, for the past 30 million years inferred from Os and Pb isotopes of a hydrogenous
326 ferromanganese crust, *Deep Sea Research Part II: Topical Studies in Oceanography* 146 (2017) 82–92.